Evaluation of the GEKO Turbulence Model for Whole Aircraft Drag Prediction

Alex Kennedy[1], Charles Stuart[2]
Trinity College Dublin, the University of Dublin, Ireland

The aim of this study was to evaluate the Generalized k-ω (GEKO) turbulence model's ability to be calibrated to improve the accuracy of the resolved drag polar for a whole aircraft geometry. The GEKO turbulence model provides a number of user configurable free parameters capable of being calibrated to better represent a given analytical setup. A global and local study was conducted on the DLR F6 geometry and validated using experimental results collected by ONERA during a wind tunnel test campaign. An ideal wind tunnel computational domain was constructed allowing for these studies to be conducted for several angle of attack design points. A calibration framework was constructed using a Box Behnken Design of Experiments (DoE) scheme to generate 21 parameter combinations, with a fine-tuning DoE scheme used to further study the influence of the parameters. A global analysis was carried out by simulating the geometry's drag polar over seven angle of attack design points, allowing for the selection of the combination of parameters that returned the highest accuracy and solver stability from the analysis of the tuning results to be examined. The effects of the GEKO model's parameters on the development of flow features and the modification of the predicted far field effects were also assessed. Further analysis was conducted using coefficient of pressure data derived from experimental results on the inboard and outboard sides of the pylon to assess the calibrated model's ability to predict the local flow field.

I. Nomenclature

AOA	=	Angle of attack (°)
BBD	=	Box Behnken Design
C	=	Mean aerodynamic chord (m)
CFD	=	Computational Fluid Dynamics
CV	=	Coefficient of Variation (-)
DNS	=	Direct Numerical Simulation
DoE	=	Design of Experiments
GEKO	=	Generalized k-ω
L	=	'Nose to Tail' length of aircraft (m)
LES	=	Large Eddy Simulation
ONERA	=	Office National d'Etudes et de Recherches Aérospatiales
RANS	=	Reynolds Averaged Navier Stokes
SST	=	Menter's Shear Stress Transport
X/C	=	X location normalized by mean aerodynamic chord length
C_{Corn}	=	GEKO corner parameter
C_{Curv}	=	GEKO curvature parameter
C_{Jet}	=	GEKO jet parameter
C_{Mix}	=	GEKO mixing parameter
C_{NW}	=	GEKO near wall parameter
C_{Sep}	=	GEKO separation parameter

[1] PhD Student, Department of Mechanical, Manufacturing and Biomedical Engineering
[2] Assistant Professor, Department of Mechanical, Manufacturing and Biomedical Engineering

C_p	=	Pressure Coefficient
D_{Far}	=	Far field Drag (N)
p	=	Pressure (Pa)
p_∞	=	Freestream Pressure (Pa)
v	=	Y-Velocity Component
v_∞	=	Freestream Velocity (m/s)
w	=	Z-Velocity Component
μ	=	Population Mean
ρ	=	Density (kg/m^3)
ρ_∞	=	Freestream Density (kg/m^3)
σ	=	Population Standard Deviation

II. Introduction

The aim of this study was to evaluate the potential of the GEKO turbulence model to be tuned by the user to generate more accurate drag predictions for a typical narrowbody aircraft. Careful selection of an appropriate turbulence model represents an integral part of the successful application of Reynolds Averaged Navier Stokes (RANS) computational fluid dynamics (CFD) analyses for a wide variety of applications, allowing companies to save both time and money that would have to be spent on experimentation. This is especially prevalent in the aviation industry where prototype testing can be extremely expensive, with wind tunnel testing costing an estimated $20,000 per hour [1]. Utilizing CFD is not without its own costs which come in the form of time, computational effort as well as the initial setup and post processing of the data generated.

Expediting the conceptual and preliminary design processes represent key enablers to facilitate progress towards complying with climate neutrality targets. Reports from organizations, such as, the International Civil Aviation Organization, state that advancements in technology will need to result in the lowering of emissions by 20% on the path to net zero [2]. This further aligns with the current view that technology improvements are essential in order for the aviation industry to reach it's 2050 [3].

An area where RANS turbulence modelling excels is for evaluating concepts generated during prototyping. Through averaging the turbulent effects of the flow, computational cost can be greatly reduced compared to both Direct Numerical Simulation (DNS) and Large Eddy Simulation (LES). Comparing grid size requirements for a Boeing wing, past work has shown RANS grids can have node counts an order of magnitude of 13 less than DNS [4, 5], which comes at the cost of receiving lower accuracy results [6]. In the conceptual design / rapid prototyping phase, there are high levels of uncertainly and a need to evaluate different concepts in a condensed timeframe which is particularly pertinent as the challenge to decarbonize the sector is driving disruptive innovation at a rate not seen in the last century. It is therefore reasonable to sacrifice the level of accuracy for a lower computational time, which matches perfectly with the area where RANS is the most effective. A persistent challenge with the application of RANS CFD relates to the choice of an appropriate turbulence model to use on the basis of knowledge or experience about the applications where that model is most effective. Depending on the scenario, this can often cause users to resort to switching models based off the scenario or concept geometry being simulated. In certain cases, attempts to resolve local flow phenomena often necessitates the use of explicit algebraic Reynolds stress models (EARSM), which are computationally intensive and less numerically stable than more traditional eddy-viscosity models. This is suitable for cases with experimental data for validating the model's performance. However, this framework for cases where this data has not been obtained, such as, creating an exploratory design tool, offers limited benefit.

The GEKO turbulence model aims to improve both the accuracy and useability of RANS turbulence modelling by giving the user access to control several "free parameters", allowing the model to be calibrated for improved flow prediction as shown in Table 1 [7]. The default version of the model mimics the flow predictions of the popular SST k-ω model. Unlike previous additions to the SST k-ω model, such as curvature correction and the reattachment modification, which are binary in nature, the free-parameters in the GEKO model can be altered across a wide range [7]. Changing the GEKO parameters modifies the underlying physics governing the flow behavior, with each parameter having been assigned a name that describes impact on the flow. For example, modifying the separation parameter, C_{Sep}, influences the eddy viscosity ratio. An increase in the C_{Sep} parameter causes a reduction in the eddy viscosity, which reduces the sensitivity of the model to adverse pressure gradients and separation [7]. By giving users this ability to tune the model by using several parameters, the GEKO model has the potential to also remove the need for switching between models and instead allowing for the flows behavior to be modified to fit the proposed scenario. The expectation is that once tuned, the GEKO model should have a good generalization capability, allowing it to adapt to any geometry for a particular application. This ability has been demonstrated previously for turbomachinery applications [8].

Table 1 GEKO turbulence model free parameters.

Parameter Name	Parameter ID	Default Value (-)
Separation	C_{Sep}	1.75
Near Wall	C_{NW}	0.5
Mixing	C_{Mix}	$C_{MixCor} = 0.35sign(C_{sep} - 1)\sqrt{(\lvert C_{sep} - 1\rvert)}$
Jet	C_{Jet}	0.90
Corner	C_{Corn}	1.00
Curvature	C_{Curv}	1.00

These traits mean that the GEKO model has the potential to vastly improve the utility of the evaluations that can be conducted in the preliminary design stage. The capacity to tune the model to better predict the flow field for a particular application enhances the ability to predict aircraft performance, allowing for a more efficient exploration of the design space. It also allows for a framework to be produced that would allow for a decrease in the time required for concept evaluation. Comparing this framework to dedicated preliminary design tools, such as, SUAVE, the computational cost will of course be higher [9]. However, while the traditional reliance on empiricism within the preliminary design process can offer rapid approximations, result accuracy is contingent upon extensive calibration of empirical and semi-empirical parameters, which can result in poor generalization capabilities [10]. Consequently, traditional preliminary design tools struggle to provide the required accuracy when used in an exploratory context, as is required in order to plot aviation's decarbonization pathway. A GEKO model enabled framework has the potential to provide a 'best of both worlds', positioning between the speed of preliminary design tools, such as, SUAVE, and higher fidelity modelling, such as, LES and DNS. The specific objectives for this study include:

- Creating an appropriate computational domain for comparing an aircraft geometry to wind tunnel testing.
- Identifying which parameters of the GEKO model are the most critical when tuning.
- Assessing how the free parameters are related to the model's performance and which parameters create the biggest gain in accuracy.
- Analyzing if the GEKO model is capable of being tuned to improve the global validation accuracy when compared to a standard SST k-ω model.
- Analysing whether the global calibration of the GEKO model generates a corresponding improvement in the prediction of local flow phenomena, which would implicitly validate an enhanced ability to reflect real flow physics relevant for commercial aircraft applications.

III. Methodology

A. Geometry & Domain

The chosen geometry for this study was the DLR F6. The DLR F6 is a representation of a modern, twin engine, narrow body, transport aircraft capable of reaching transonic speeds. It was originally developed in the 1980s based off the older DLR F4 geometry [11]. The 3D half geometry model version used in the AIAA's 2nd Drag prediction workshop was selected. As a part of the original test campaign conducted by ONERA, several nacelle configurations were tested. The version used for this study was the CFM56-Long Nacelle in position 1, as defined in the original AIAA study [12].

A solid aircraft model was produced from the surface geometry provided by the AIAA [12]. Using the surface features available in *SolidWorks,* an imprint of the plane model was able to be derived which allowed for the creation of a full aircraft model. To create the desired design point, the geometry was rotated about the aircraft's centerline, adjusting the pitch of the model relative to the axis of the fluid flow according to the Angle of Attack data provided from the ONERA test campaign [13]. Once the model had been adjusted to the desired angle of attack, the enclosure feature within ANSYS SpaceClaim was utilized to produce the surrounding domain. Through an iterative process utilizing several SST k-ω simulations, a sizing scheme was developed by examining the flow features and gradients surrounding the aircraft geometry and expanding the domain to capture both the surface and far field flow effects of the geometry. Particular care was taken to resolve the wind tip vortices in both the spanwise and streamwise directions to ensure accurate prediction of far field effects. The final sizing dimensions were then normalized by the aircraft geometry's dimensions, as illustrated in Fig. 1.

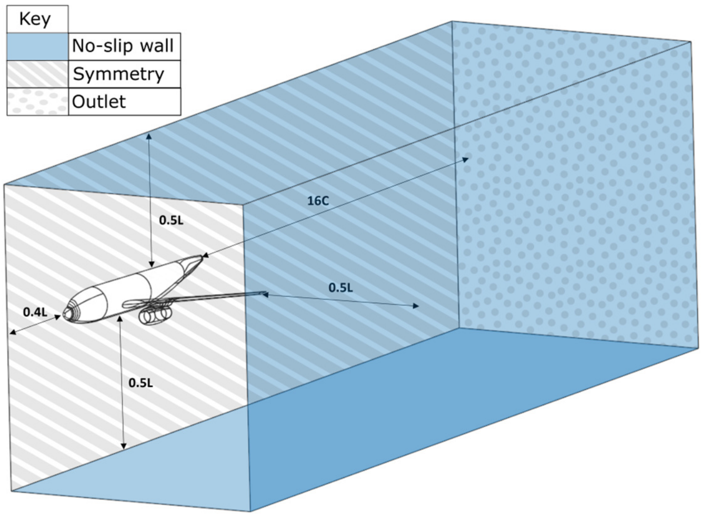

Fig. 1 Sizing scheme and boundary conditions of the computational domain.

B. Numerical Setup

The SST k-ω model was used as a control to understand the expected error generated from the current industry standard model. The predictions generated by the SST k-ω model also represent the baseline behavior of GEKO model, i.e. with the GEKO parameters set at the default values (as depicted in Table 1). Once the initial control results were generated, the second phase of the work consisted of setting the GEKO parameters based off the combinations generated from the design of experiments scheme. Each parameter combination was simulated at an angle of attack (AOA) of 1.738° with the selection criteria for the tune used for comparison against the SST k-ω model based off the accuracy of the result at this design point. The hypothesis behind using a higher AOA rather than a lower AOA is based on the principle that RANS turbulence modelling accuracy is generally inversely proportional to the complexity of a flow scenario, as was the case for the grid independence study. More complex scenarios will yield reduced accuracy while more conventional flows will be resolved with a greater accuracy. Using this understanding of RANS turbulence modelling, in theory, tuning from a design point that creates a more complex flow scenario, any increase in model accuracy in this scenario should result in further gains in model accuracy at design points with lower AOAs, which generate more straightforward flow structures.

To analyse the results of each parameter combination and assess whether that combination had increased or decreased the model's accuracy relative to the experimental results, total error was assessed. This was the sum of the percentage error between the surface drag coefficient results and the surface lift coefficient results. Depending on the parameter setup, certain tunes were seen to positively affect correlation for the drag coefficient values while negatively affecting the error for the lift coefficient and vice versa. Therefore, evaluating each tune based off the total error achieved a more balanced parameter for assessing overall performance.

The specified values for the boundary conditions and reference values were established according to the conditions recorded during the wind tunnel test campaign. A large portion of the provided data was recorded for a Mach number of 0.75 with a Reynolds number of approximately three million. The mean parameter values for the wind tunnel, shown in Table 2, were recorded during the AOA sweep tests conducted at ONERA. These values were used for setting the boundary conditions of the domain and informed the meshing approach used, such as, 1st cell height. These values, as well as the recorded static temperature of 274K were then utilised to define the air fluid properties, with a density of 1.478 kg/m^3 and a dynamic viscosity of 1.7×10^{-5} kg/ms.

Table 2 Wind Tunnel Test Values.

Parameter	Value
Mach	0.750
Stagnation Pressure (Pa)	168872.98
Static Pressure (Pa)	116281.66
Stagnation Temperature (K)	305.10
Reynolds number	3.01×10^6
Area (m^2)	0.0727
Density (kg/m^3)	1.47873
Length (m)	0.14547
Pressure (Pa)	116372.8
Temperature (K)	274.157
Velocity (m/s)	248.925
Viscosity (kg/ms)	1.72×10^{-5}
Ratio of Specific Heats	1.4
Yplus for Heat Tran. Coef.	300

The turbulence intensity of the model was set at 1.7% based off previous research conducted to assess the turbulent characteristics of the S1MA wind tunnel used by ONERA [14]. The operating pressure in the domain was set according to the static pressure of 116281.66 Pa, this applies an initial global value to all fluid zones. A symmetry boundary condition and no-slip wall boundary condition was applied to the symmetry and tunnel walls named selections, respectively. At the outlet face of the wind tunnel domain a pressure outlet was set, with the turbulent intensity and length scale in line with the inlet conditions. A value of 0 was adopted as the gauge pressure, which applies this value to all the cells at the inlet, due to formula ANSYS utilizes for absolute pressure calculations [15].

C. Meshing Scheme

The meshing process itself was conducted within ANSYS Fluent Meshing to utilize its polyhedral volume mesh feature. Due to the nature of the problem being discussed it was necessary to obtain a mesh that was both of acceptable quality and of a relatively low cell count to fit the rapid prototyping profile. Due to the smaller features and curved surfaces of the DLR F6 geometry, for a Y+ ≤ 1 to be achieved across the entire model for the given setup, a minimum mesh resolution of 12 million cells would have been required. As the computational time and resources would not have fit within the target for the study background, the boundary layer mesh was setup to produce an average Y+ of < 2 across the DLR F6 geometry. It can be seen from previous work that this is not an unconventional practice, particularly in 3-D aircraft models, with Y+ values often varying between 2-10 for low resolution grids [16-18].

Once the necessary boundary layer was established, and the surface mesh was at a resolution to accurately capture the surface of the aircraft geometry, a grid refinement study was conducted for the volume mesh of the surrounding domain. For the grid refinement study the skin friction drag coefficient of the DLR F6 was used to assess the convergence of the meshes. To ensure the mesh would be converged across a drag polar rather than a single design point, the study was conducted for two AOAs, the first study at 1.738° and the second at 0.190°. Both of these AOAs had experimental results from the AOA sweep test conducted in the ONERA wind tunnel [13].

The mesh was first refined for the higher AOA before being re-verified for the lower AOA. This was based on the knowledge that a higher AOA would produce steeper gradients and more complex flow features to resolve and as such would require more refinement than a lower AOA. The mesh was refined using the standard Richardson extrapolation method [19, 20]. An approximate refinement factor of 2 was implemented across each mesh which led to the creation of a coarse, medium and fine mesh with approximately 3 million, 6 million and 12 million cells respectively. In order to maintain a mesh of sufficient skewness and orthogonality, the boundary layer first cell height for the coarse mesh was raised to allow the quality to be maintained across all meshes. This gave a corresponding y+ value of ≤ 5.

Each mesh was validated for a simulation of 250 iterations, which was a sufficient number of iterations for the residuals to reach steady state as discussed in Section B. Simulations were carried out using an Intel Xeon w5-2465X

16 core processor. Parallel solver processes were enabled with the MPI function set to 'intel' to reduce computational time. The full results for both studies are shown in Table 3 below.

Table 3 Results from grid independence studies.

Mesh	Solution Time (mins)	C_D	Extrapolated Error (%)	GCI^{21}_{fine} (%)
Test 1 – AOA 1.738				
Coarse	165	0.03339	17.27	
Medium	618	0.03154	10.81	
Fine	1470	0.03039	6.76	2.11
Extrapolated Value		0.02847		
Test 2 – AOA 0.190				
Coarse	214	0.02836	18.45	
Medium	491	0.02661	11.16	
Fine	1396	0.02556	6.75	1.95
Extrapolated Value		0.02394		

Plotting these results graphically, as shown in Fig. 2, it can be seen the mesh converges towards the zero-grid spacing extrapolated value and how the solution time increases significantly with each step of mesh refinement.

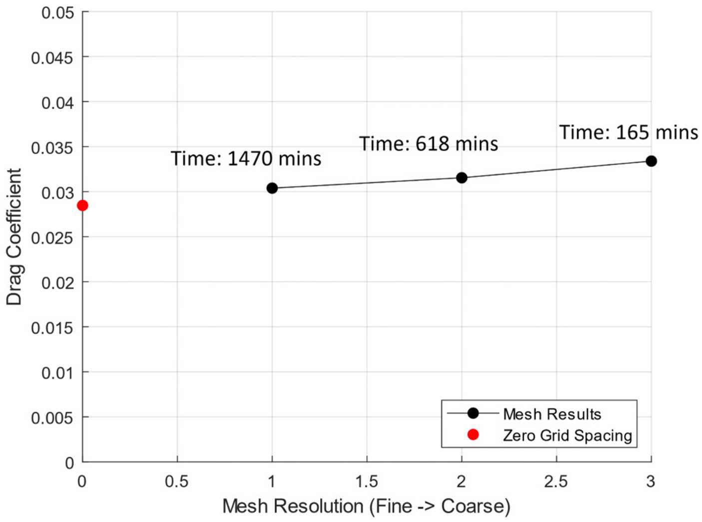

Fig. 2 Grid refinement study results for AOA 1.738 design point.

Based off the GCI results, it can be seen that the solution running time for the fine mesh is an order of magnitude greater than the medium mesh. Despite the lower resolution of the medium mesh, both meshes maintained a y+ ≤ 2 while having an acceptable quality. The quality thresholds applied for the mesh to be deemed acceptable included achieving a minimum orthogonality above 0.1, an average orthogonality above 0.95, while keeping maximum skewness below 0.9 and an average skewness below 0.25.

Although there is a difference in the extrapolated error between the medium and fine meshes, the usability of the model must also be considered. The nature of this study requires a significant number of simulations to be completed. The estimated uncertainty of the C_D recorded in the ONERA wind tunnel at the time of the experimental measurement, is estimated to be approximately 7.4% [13, 21]. Considering this uncertainty along with the fine mesh requiring over double the simulation time, it would not be feasible to use this mesh. The significant time constraints of the project, the number of simulations required, the overall quality and corresponding y+ of the mesh as well as the time to complete a simulation using that mesh were all key factors that contributed to the decision to proceed with the medium mesh. By keeping the discretization error low, a higher confidence that the mesh would not be a significant factor to the results acquired from the CFD study was achieved.

D. GEKO Tuning Framework

For creating the tuning framework, a key aspect that was considered when deciding on which scheme to select for the tuning phase was the overall stability and usability of the ANSYS solver. Due to the GEKO free parameter values directly influencing the turbulence models performance and thus forming a critical aspect of the model's setup, if values were configured in a way that could cause the simulation to diverge, this could cause a loss of results and valuable simulation time. Due to the appetite to reduce the number of parameters situated at the end points of their respective value ranges at one time, it was decided that a relatively conservative testing scheme would be utilized. A Design of Experiments (DoE) framework was employed to allow for multiple inputs to be used at one time to determine the influence and interaction of the parameters on the desired outcome and to reduce the number of tests required compared to a normal experimental campaign. These benefits, along with the need to reduce the number of parameters at their respective end points or 'corner point' of their value ranges at one time, led to the selection of the Box Behnken design (BBD) DoE method for this process. The BBD method requires three value levels for the parameters being studied. The BBD scheme can be described as having 'missing corners,' as shown in Fig.3, which can be useful in cases where extreme combinations of several parameters should be avoided to improve the solver stability [22].

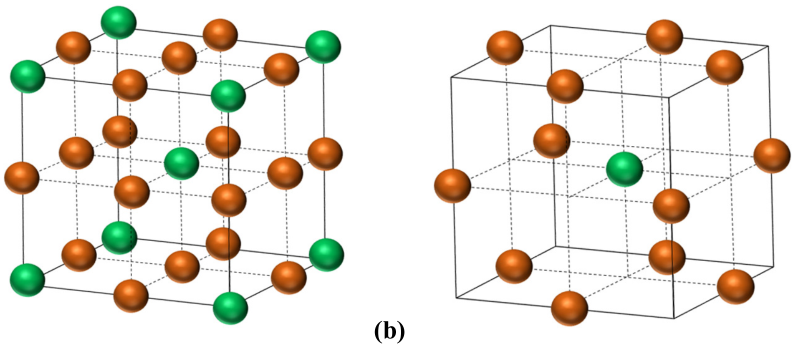

(a) (b)

Fig. 3 Comparison of (a) Full Factorial and (b) Box Behnken sampling approaches (adapted from [22]).

Due to the relationships between the parameters, it was necessary to consider which selection would offer the highest return from being tuned. Several coefficients can be defined relative to the values for other parameters. An example of this can be seen with the mixing variable, C_{Mix}. This value can be set using Eq. (1), an ideal formula that ANSYS has created [7]:

$$C_{MixCor} = 0.35\,\text{sign}(C_{Sep} - 1)\sqrt{(|C_{Sep} - 1|)} \tag{1}$$

Due to the mixing parameter's ability to be correlated to the C_{Sep} parameter, to simplify the testing campaign and the number required experiments, this formula was used to determine the value for C_{Mix} for all tests.
The other parameter which was considered more complex to tune when compared to other parameters is the C_{Jet} variable. The jet parameter was created for more specific flow scenarios with its main applications based around fluid jets, such as, round or plane jets. ANSYS recommends that the C_{Sep} parameter must be within the range of 1.75-2, otherwise C_{Jet} will not have a strong enough effect to achieve the desired results [7]. Due to the caveats that exist for the C_{Jet} parameter and ANSYS themselves stating that for majority of cases, C_{Jet} can be left at its default value of 0.9, this parameter was considered a confounding variable and was fixed throughout the tuning study.

In past work conducted by ANSYS relating to the assessment of the GEKO turbulence model's impact for external flow scenarios, specifically on wing geometries, accuracy has been shown to increase when C_{Sep} is set in the range 2-2.5 [7]. The knowledge gained from this past work, as well as the fact that for this study, the tuned model will be directly compared to the SST k-ω model, contributed significantly to selecting the parameter value ranges. Since the SST k-ω model is equivalent to the GEKO model with default parameters (which uses a C_{Sep} value of 1.75), the range for C_{Sep} was set to 2-2.5. The remaining parameter value ranges for the tuning process were set according to the minimum, mid-range, and maximum values (corresponding to -1, 0 and 1, respectively) shown in Table 4. Using these specifications, a BBD DoE table was constructed which consisted of 21 tuning experiments each with a unique value combination of the GEKO parameters. These parameter values used for each test can be seen in Table 5.

Table 4 GEKO turbulence model free parameters tuning value ranges.

GEKO Parameter	-1	0	1
C_{Sep}	-	2	2.5
C_{NW}	0.5	1.25	2
C_{Curve}	0.5	1	1.5
C_{Corn}	0.5	1	1.5
C_{Mix}	$C_{MixCor\ (Eq.1)}$	$C_{MixCor\ (Eq.1)}$	$C_{MixCor\ (Eq.1)}$
C_{Jet}	0.9	0.9	0.9

Table 5 GEKO turbulence model tuning parameter combinations.

	Parameter Set	C_{Sep}	C_{NW}	C_{Curv}	C_{Corn}	C_{Mix}	C_{Jet}
Block 1	1	2.5	1.25	1.5	1.5	0.4	0.9
	2	2.5	2	1.5	1	0.4	0.9
	3	2.5	1.25	0.5	0.5	0.4	0.9
	4	2	1.25	1.5	1	0.4	0.9
	5	2.5	2	0.5	1	0.4	0.9
	6	2	1.25	1	0.5	0.4	0.9
	7	2.5	1.25	0.5	1	0.4	0.9
Block 2	8	2.5	1.25	1	1	0.4	0.9
	9	2.5	2	1	0.5	0.4	0.9
	10	2	1.25	1	1.5	0.4	0.9
	11	2.5	0.5	1	1.5	0.4	0.9
	12	2	0.5	1	1	0.4	0.9
	13	2.5	0.5	1.5	1	0.4	0.9
	14	2.5	1.25	1	1	0.4	0.9
Block 3	15	2	2	1	1	0.4	0.9
	16	2.5	1.25	1.5	0.5	0.4	0.9
	17	2.5	1.25	1	1	0.4	0.9
	18	2.5	0.5	1	0.5	0.4	0.9
	19	2	1.25	0.5	1	0.4	0.9
	20	2.5	0.5	0.5	1	0.4	0.9
	21	2.5	2	1	1.5	0.4	0.9

Once the initial study had been completed, the results were analysed to find a range of values which could be used for fine tuning work. A further DoE scheme was produced for these fine-tuning experiments with the aim of further assessing the characteristics and interactions between the GEKO free parameters. This led to an additional thirteen simulations, with smaller steps between values for each of the parameters used for the initial GEKO tuning DoE. To produce the second DoE scheme, each parameter was assigned a smaller range based off the initial tuning results, the step between values was then set to 0.15, reducing it from the 0.5 value used for the first scheme as shown in Table 6.

Table 6 Second DoE scheme for GEKO fine tuning.

Parameter Set	C_{Sep}	C_{NW}	C_{Curv}	C_{Corn}	C_{Mix}	C_{Jet}
22	2.15	1.25	0.65	0.8	0.4	0.9
23	2.45	1.25	0.65	0.8	0.4	0.9
24	2.15	1.25	0.95	0.8	0.4	0.9
25	2.45	1.25	0.95	0.8	0.4	0.9
26	2.15	1.25	0.8	0.65	0.4	0.9
27	2.45	1.25	0.8	0.65	0.4	0.9
28	2.15	1.25	0.8	0.95	0.4	0.9
29	2.45	1.25	0.8	0.95	0.4	0.9
30	2.3	1.25	0.65	0.65	0.4	0.9
31	2.3	1.25	0.95	0.65	0.4	0.9
32	2.3	1.25	0.65	0.95	0.4	0.9
33	2.3	1.25	0.95	0.95	0.4	0.9
34	2.3	1.25	0.8	0.8	0.4	0.9

E. Analysis Setup

1. Drag Polar

To assess the accuracy of the model, several levels of analysis were used. Firstly, the results for each model were compared globally through their drag polar curves. For both the SST k-ω and the tuned GEKO model, seven AOAs were simulated in order to produce full drag polar curves. These results were evaluated against the experimental data recorded from the angle of attack sweeps conducted during the ONERA test campaign. To generate the lift and drag coefficient at each design point, each simulation was run until its residuals converged. For challenging operating points, this occasionally corresponded to a periodic oscillation. While such a pattern is indicative of the presence of unsteady effects, given the focal point on contributing towards a preliminary design tool, the decision was taken to maintain the use of a steady state calculation (rather than switching to a computationally demanding URANS-based approach). In such circumstances, once the residuals began to exhibit periodic behavior, five cycles were simulated, where the variation from the mean C_D value was below ten drag counts, to generate a mean value for the drag and lift coefficients. An example of this convergence can be seen in Fig. 4, where it can be seen that the residuals required approximately 100 iterations before converging on a repeating cycle. Several cycles were then simulated in order for a mean for each result to be obtained.

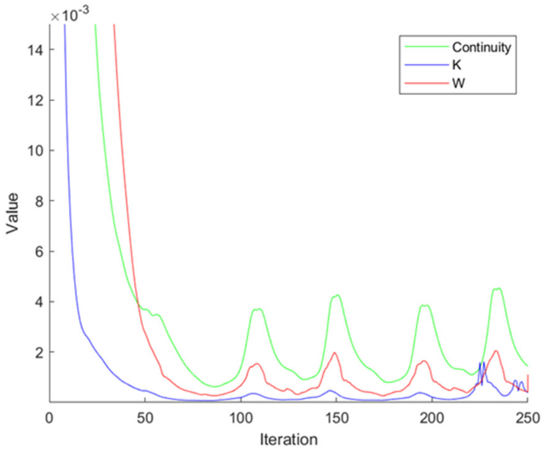

Fig. 4 Example of steady state residual pattern.

2. Pressure Taps

To thoroughly assess the model's performance, results were also compared on a local level, using the static pressure taps and recorded pressure data from the ONERA test campaign. Several numerical monitor points, corresponding to the locations of the experimental pressure taps, were placed along the aircraft's pylon to analyse the flow features present in this region. The coordinates for several of these pressure taps were provided by ONERA at an AOA of 0°. Using these coordinates as outlined in Table 7 the local flow predictions of the model were compared to experimental results [13].

Table 7 Pylon pressure tap coordinates at AOA 0°.

No.	X (mm)	Y (mm)	Z (mm)
61	37	206.31	12.62
62	56	206.66	13.95
63	77	207.03	15.42
64	97	200.42	9.5
65	97	214.22	9.5
66	116	200.75	7.5
67	116	214.55	7.5
68	170	202.32	2
69	170	214.8	2

ONERA provided the pressure tap data recorded for three, angles of attack, specifically 1.738°, 1° and 0.190°. To assess the performance of the model locally, the experimental pressure tap data was compared to numerical monitor point data for the AOA of 1.738°. To implement the coefficient of pressure formula within ANSYS, a custom variable was made for Eq. (2) within ANSYS CFD Post to allow the coefficient of pressure to be produced for each monitor point [23]. This allowed the coefficient of pressure to be directly converted from the simulation pressure data.

$$C_p = \frac{p - p_\infty}{\frac{1}{2}\rho_\infty v_\infty{}^2} \tag{2}$$

In order to correct the coordinates of the monitor points / pressure taps when moving between the different AOA values, the coordinates were geometrical rotated about the y coordinate plane or the pitch axis of the aircraft. Using this assumption, the new coordinate points could be generated through rotation about a 2-D plane. Once the new coordinates were converted for the AOA 1.738° design point, the taps were fitted to the DLR F6 geometry within ANSYS CFD Post as shown in Fig. 5.

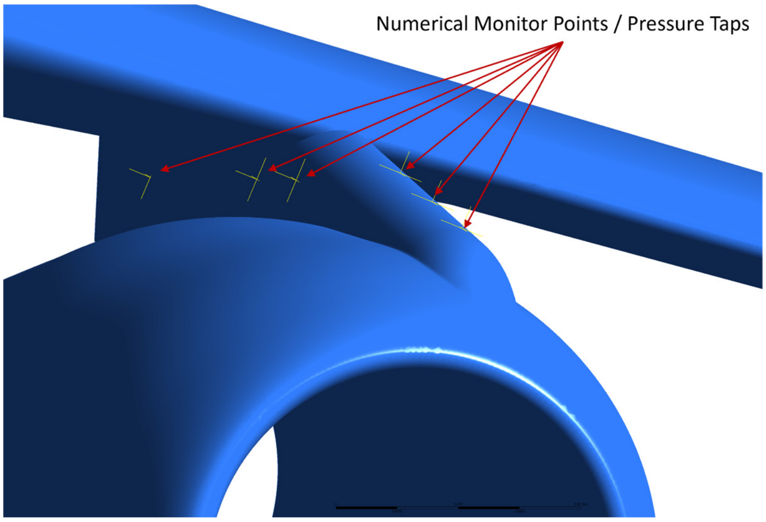

Fig. 5 Pressure taps on pylon for AOA 1.738.

3. Trefftz Plane

To assess the changes to the induced drag generated by the alterations to the turbulence model, the Trefftz plane method was utilised. To assess the far field impact of induced vortices, planes were placed at intervals of length C behind the wing of the aircraft geometry to assess the distance required for the vortices to dissipate and re-merge with the freestream flow. In total 16 measurement planes were setup, as shown in Fig. 6. As with the coefficient of pressure, a custom user function was used within ANSYS Fluent. At each plane, an induced drag measurement was made by taking a surface integral of the velocity vectors acting non-parallel to the flow. Each result was then multiplied by half the density as in Eq. (3).

$$D_{Far} = \frac{\rho}{2} \iint_{S_T} (v^2 + w^2)\, dS \tag{3}$$

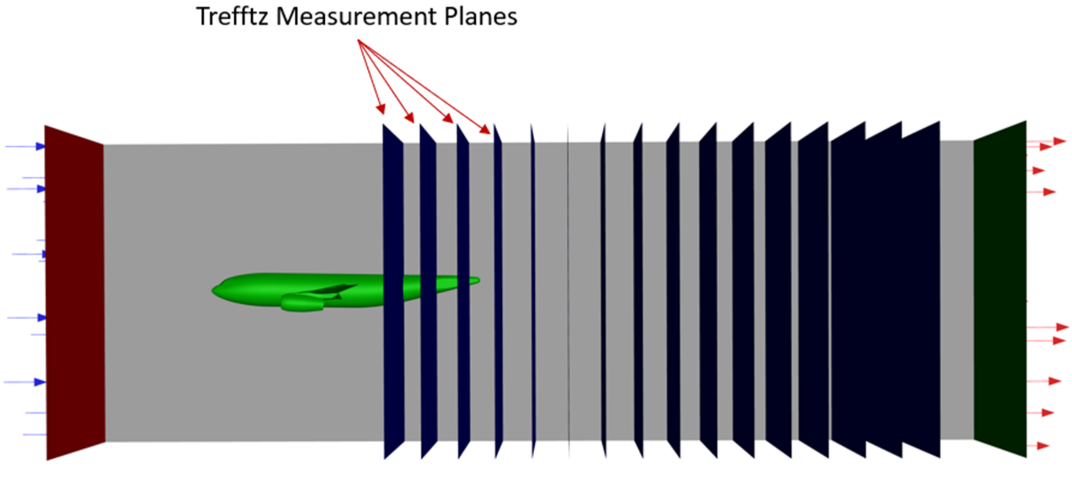

Fig.6 Trefftz planes set at intervals of length C between trailing edge and outlet.

IV. Results

A. Tuning Results

1. *Initial Tuning Results*

From the completed tuning test results, it can clearly be seen that changing the variables resulted in a corresponding variation in the model's predictions of lift and drag. Out of the 21 tests conducted, nine of those parameter combinations resulted in a gain in overall accuracy when compared to the SST k-ω model's predictions for the AOA 1.738° design point. As shown in Fig. 7, for certain parameter combinations, it was observed that a significant gain in one coefficient's accuracy, such as the lift coefficient, would cause a decrease in accuracy of the drag coefficient. This would result in an overall higher error when compared to the SST k-ω model.

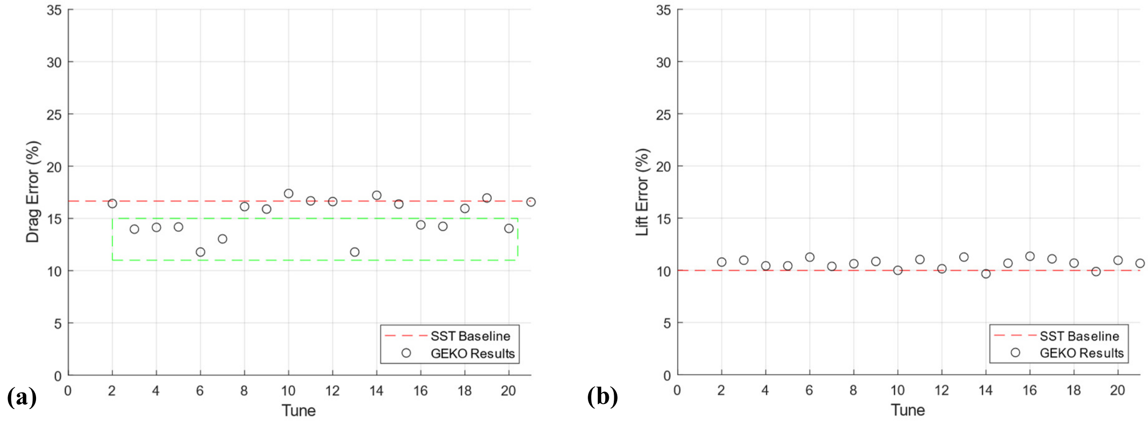

Fig. 7 Error across each GEKO parameter combination for (a) drag and (b) lift coefficient.

For the AOA 1.738° design point the SST k-ω model returned a 16.66% error in the drag coefficient value and a 10% error in the lift coefficient error. It was evident from the results of the tuning that the various combinations of parameters have a significant effect on the result accuracy, with the highest accuracy predicting a drag coefficient within 47 drag counts of the experimental result, while the lowest accuracy returned a drag count difference of 71. The results for the top five tuning combinations for the 1.738° design point are shown in Table 8.

Table 8 Parameter combinations of the top five tuning results.

Tune	C_{Sep}	C_{NW}	C_{Curv}	C_{Corn}	Drag Error (%)	Lift Error (%)
Tune 4	2	1.25	1.5	1	14.14	10.43
Tune 7	2.5	1.25	0.5	1	13.04	10.38
Tune 13	2.5	0.5	1.5	1	11.78	11.27
Tune 6	2	1.25	1	0.5	11.78	11.26
Tune 16	2.5	1.25	1.5	0.5	11.83	11.11

2. *Fine Tuning Results*

As discussed in Section III Part D, based off the results from the initial tuning work, a second set of DoE tests was created as shown in Table 6. The bounds for the value ranges within this new framework were established based off the results from the top five tuning results from the initial tuning scheme. The results from the design of experiment scheme, illustrated in Fig. 8, highlight that 12 out of 13 of the fine-tuning schemes improved marginally on the SST k-ω result. However, none of the fine-tuning schemes improved upon the performance of the top five tunes in Table 8. These results provide an indication of the robustness of the GEKO model once a range of improvement for the GEKO values is identified. When tuning the parameters in smaller intervals within set bounds, the results are not particularly sensitive to small parameter changes (which may be indicative of good generalisation capability), while still allowing for the facilitation of flow modifications.

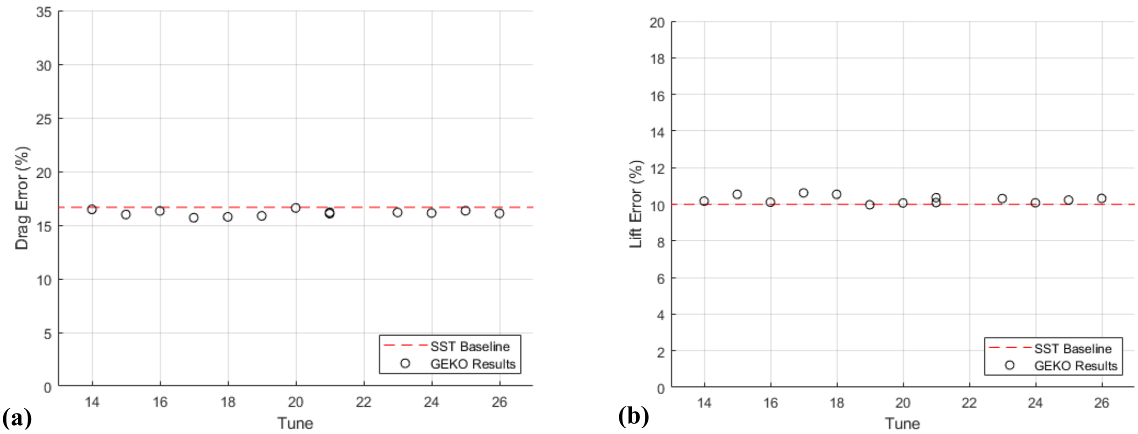

(a) (b)

Fig. 8 Error across GEKO parameter fine tuning scheme for (a) drag and (b) lift coefficient.

Once the results from the tuning schemes had been assessed for an AOA of 1.738°, GEKO parameter combination seven was selected for further analysis against the SST k-ω model on a global level over seven design points. The ability of the calibrated GEKO model to accurately predict local flow features was also compared to the capabilities presented by the baseline SST k-ω model.

3. Solver Stability

Once the tuning DoE studies were completed, the coefficient of variation (CV) associated with the converged solver residuals for each of the parameter combinations was examined. The rationale here was to study the impact of tuning the GEKO parameters on the amplitude of the periodic solver residual oscillations (as described in Section III Part E), and hence to ascertain whether there was a link between drag prediction error and solver stability. The AOA was maintained at 1.738° as with the tuning simulations. To examine the change in oscillations, the value of drag coefficient was selected to be studied across four cycles as in Fig. 4. The equation used to evaluate CV is depicted in Eq. (4), where σ and μ refer to the population standard deviation and mean, respectively.

$$CV = \frac{\sigma}{\mu} \tag{4}$$

It was found that the maximum CV was 0.018 while the minimum value was 0.005. Together with the rest of the results depicted in Fig. 9, the range of CV values encountered clearly illustrates that modification of the GEKO parameters had a tangible impact on the stability of the solver. While the results indicate a general increase in drag prediction error with increasing CV, no definitive link was found (exemplified by a relatively low linear regression R^2 value of 0.4). However, it was seen that parameter combinations that had a high curvature (C_{Curv}) and separation value (C_{Sep}), while being assigned near wall (C_{NW}) and corner (C_{Corn}) parameters of unity (which represents a low-to-midrange value), experienced the highest stability. Ultimately, it was noted that four out of the five lowest coefficient of variance cases had been assigned this type of parameter combination. The results presented demonstrate that the parameter combinations that sought to reduce flow separation / recirculation extent implicitly suppressed unsteady flow effects, yielding a reduction in residual oscillation amplitude for the steady-state RANS solver used in this study. This is in line with previous expectations associated with increasing the C_{Curv} and C_{Sep} values [7]. This observation is further underpinned upon examining the impact of the changing the GEKO free parameters on local flow features, as is explored in further detail in Section IV Part A.4.

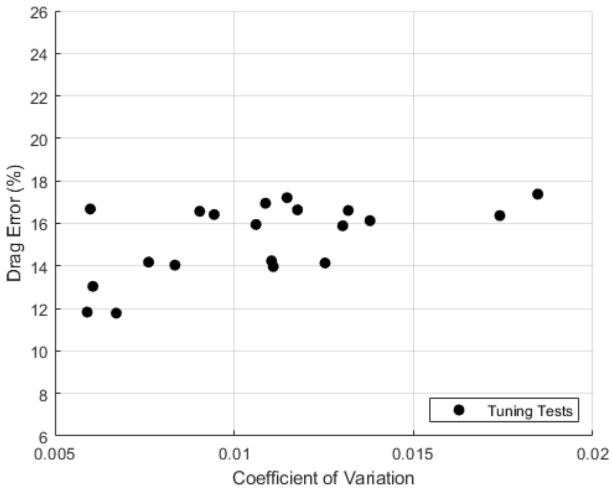

Fig. 9 Coefficient of Variation results for tuning tests.

4. Modification of local flow features

In order to assess the localized effects of the GEKO model's free parameters, a commonly observed flow feature was chosen to observe the modification potential at an AOA of 1.738°. The chosen flow feature was the re-circulation that occurs at the rear of the plane body-wing junction as shown in Fig.10. The first parameter that was examined was the GEKO model's corner parameter. The comparisons shown in the figures below were conducted using identical streamlines and user bounded static (gauge) pressure contours. For each comparison study, two tunes that maintained the same parameter values besides the parameter being studied, were selected.

For comparing the corner parameter, GEKO Tune one and Tune sixteen were compared, with Tune one having a corner parameter of 0.5 against a value of 1.5 for Tune sixteen. From Fig.10, it can be seen that the lower value corner parameter of Tune one, shows a significant reduction in the extent of the re-circulating region compared to the higher value of Tune 16. The higher-pressure region that develops on the wing before the separation of the flow from the wing is predicted to be of a lower magnitude for the lower corner parameter. The pressure drop that occurs due to the re-circulation is estimated to be larger when the corner parameter is at a higher value. This is in line with expectations set by ANSYS, which demonstrated that raising the corner parameter can increase the pressure locally [7].

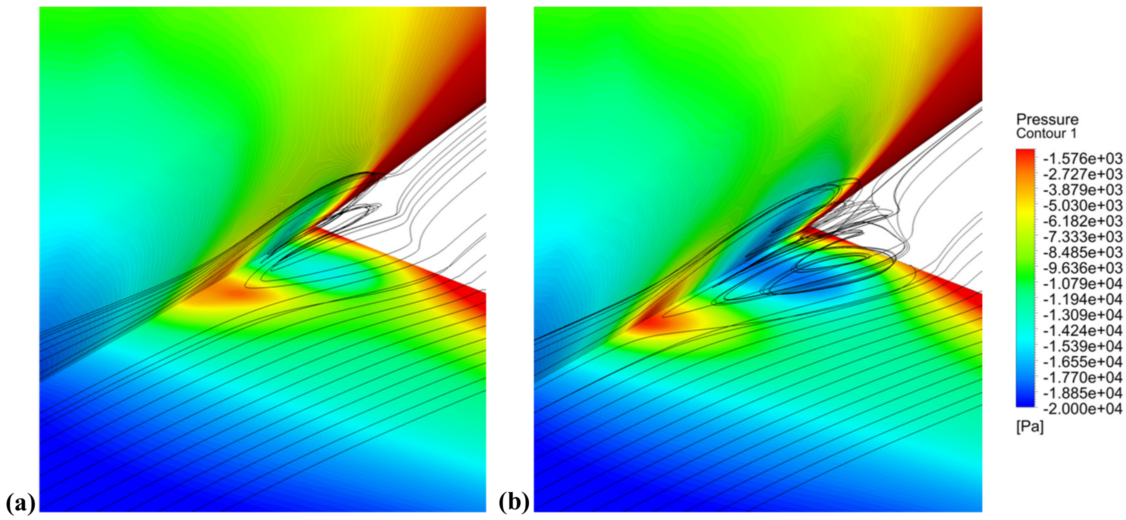

Fig. 10 Corner parameter flow feature comparison (a) Tune 1 and (b) Tune 16.

Examining Fig. 11 which compares the effect of changing the curvature parameter, it can be seen that the opposite trend is illustrated. Tune two which has a curvature value of 1.5 demonstrates a reduction in the size of the re-circulation region compared to the lower 0.5 value of Tune five. However, Tune two also indicates a larger vortex shed from the wing compared to the Tune five, indicating a later separation of the flow from the wing. The spanwise extent of the re-circulation region along the wing is also reduced. However, the vortex appears to be of a higher intensity. The aim of the curvature correction term is to handle the effect of swirl and rotation [7]. Therefore, the increased curvature value of Tune two alters the expected intensity of the swirl predicted at the aft of the wing body junction.

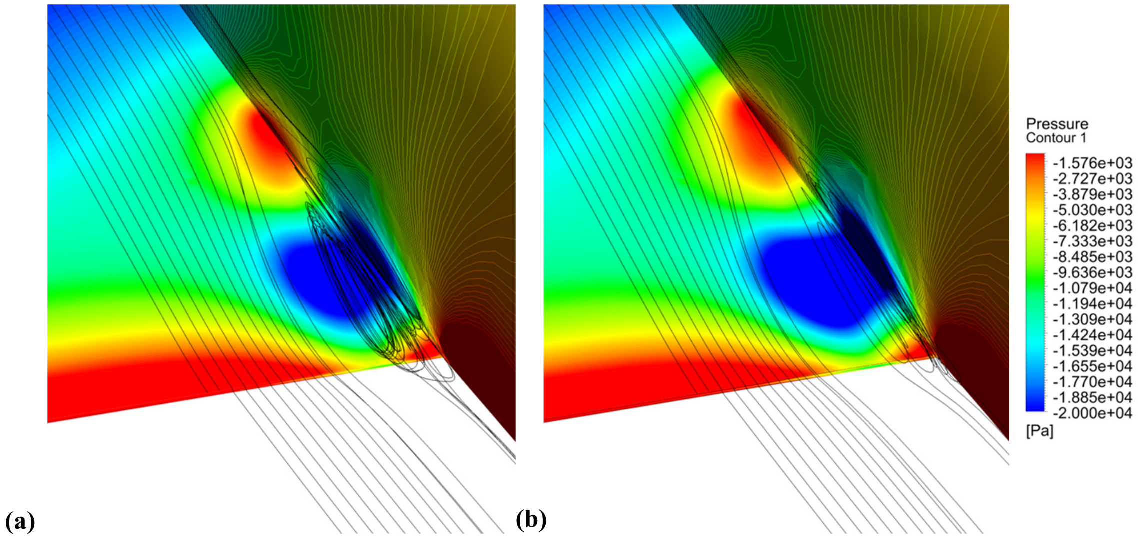

Fig. 11 Curvature parameter flow feature comparison (a) Tune 2 and (b) Tune 5.

Examining the effects of the separation parameter shown in Fig. 12, it can be seen that as the separation value is increased, the predicted size of the re-circulation is reduced, as well as the magnitude of the higher and lower pressure regions that occur on the wing. Tune seven, which has a separation parameter of 2.5, shows a significant reduction with only a minor parameter modification compared to Tune 16, which has a parameter value of 2. This highlights the intended design of the C_{Sep} parameter as the higher value reduced the model's sensitivity to adverse pressure gradients, creating this reduction in separation extent. This significant change in the flow from a minimal value change also aligns with the expectations set by ANSYS, that the C_{Sep} parameter has the greatest impact on the model results and demonstrates why this parameter should be modified before tuning other parameters.

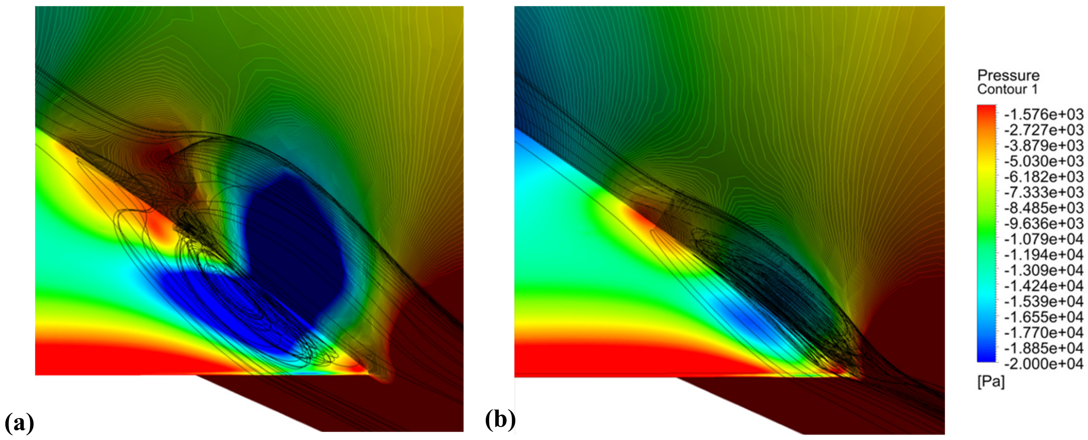

Fig. 12 Separation parameter flow feature comparison (a) Tune 19 and (b) Tune 7.

A similar result can be seen when examining the effects of modifying the near wall parameter (C_{NW}) in Fig.13, as the value assigned to the parameter increases, the separation region is reduced in size. Comparing Tune 12, which has an assigned value of 0.5, to Tune 15 with a value of two, a reduction in the spread of the streamlines can be observed. The near wall parameter demonstrates a stronger effect near the wall region, while returning a lower modification as a result to changes in value. While the C_{Sep} parameter effects the entire boundary layer, the C_{NW} parameter alters only the inner part of the velocity profiles at non-equilibrium regions [7].

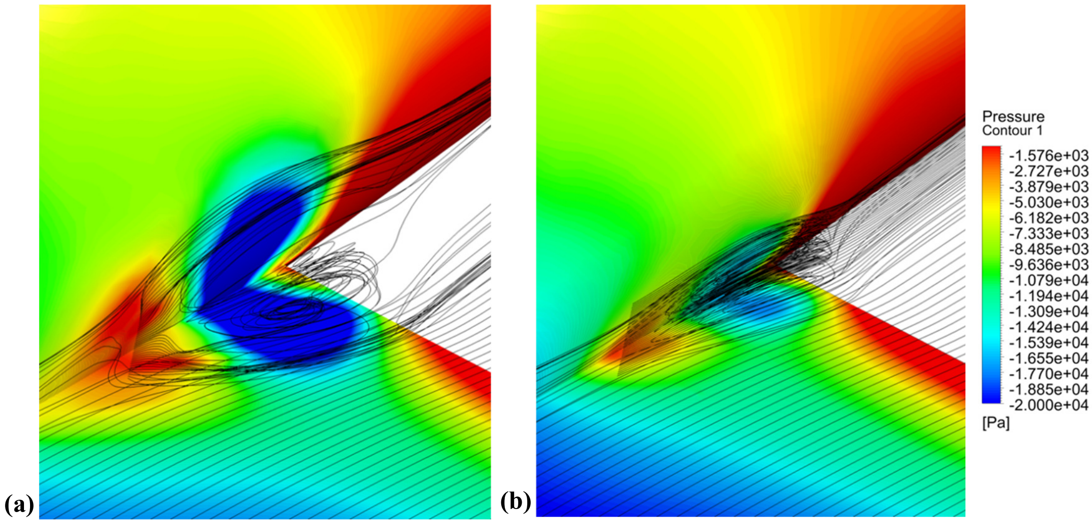

Fig. 13 Near wall parameter flow feature comparison (a) Tune 12 and (b) Tune 15.

From the results for the GEKO model at an AOA of 1.738, in Fig. 14 (a), it can be seen that the tuned model (Tune 7) no longer predicts the sharp negative pressure gradient previously detected by the SST k-ω, as shown in Fig. 14 (b). Instead, a much smoother pressure contour can be observed. A known limitation of the SST k-ω turbulence model is it's overprediction of separation regions when operating in adverse pressure gradients. The calibrated GEKO model predicted a significantly smaller recirculation region compared to the SST k-ω model, which is more in line with the flow visualization results from the ONERA test campaign shown in Fig 15. It can also be seen that the GEKO model predicts the flow feature to develop significantly further 'aft' or rearward on the wing geometry which was also seen in the wind tunnel testing. These differences are easiest to compare using a top-down view as in Fig 15.

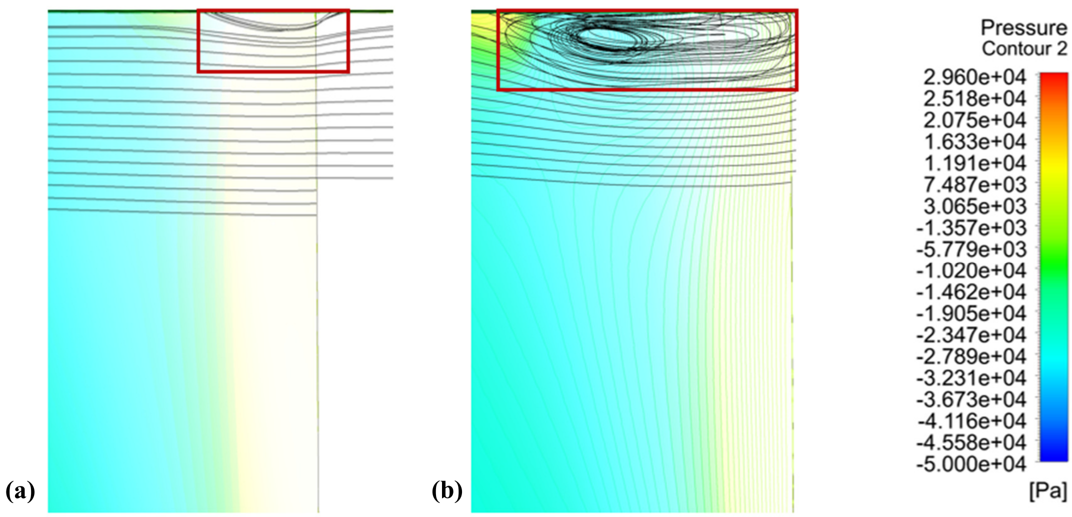

Fig. 14 Wing body junction flow visualization results for (a) GEKO and (b) SST k-ω top-down view.

Fig. 15 Wing body junction flow visualization results top-down view ONERA wind tunnel test.

5. Far Field

To study the effects of the GEKO model on the flow in the wake of the aircraft geometry, a far field study was conducted for several tunes using the Trefftz planes depicted in Fig. 6, where plane one is leftmost in the diagram. The results of the analysis are illustrated in Fig. 16. It can be seen that the SST k-ω model predicted a greater induced drag across all measurement points, while Tune nine predicted the lowest induced drag.

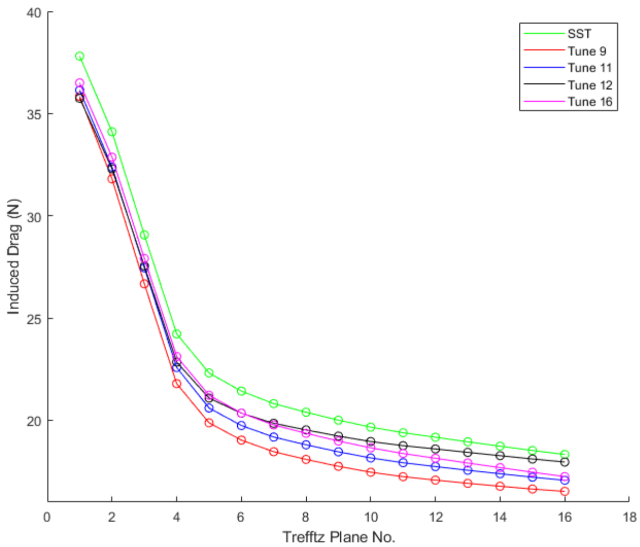

Fig. 16 Comparison of GEKO effect on far field drag.

By examining the vorticity magnitude at Trefftz plane one and plane four, as shown in Fig. 17 and Fig. 18, it can be seen that initially Tune nine and the SST k-ω model predict comparable results, with the vortex strength aft of the wing body junction illustrating marginal differences. However, Fig. 18 clearly shows as the flow travels further downstream, the difference in the predicted vortex strength between the two models becomes increases significantly.

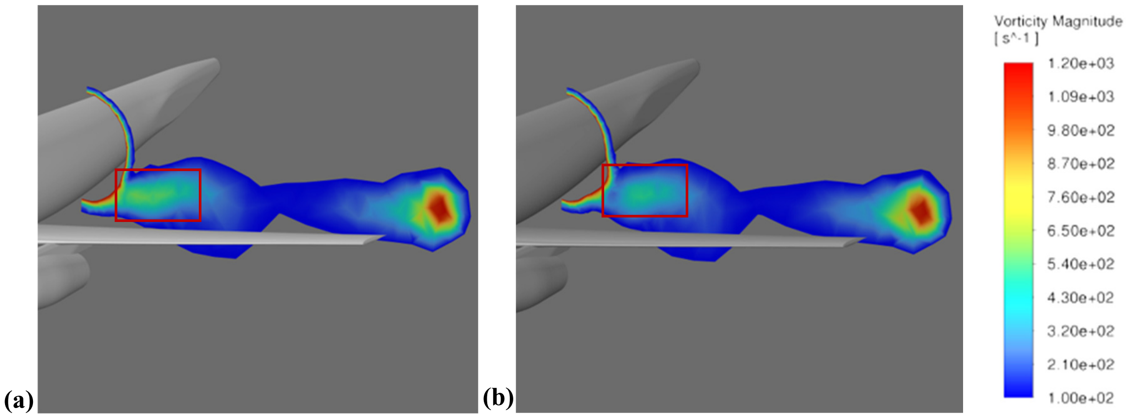

Fig. 17 Vorticity magnitude comparison on Trefftz plane 1 (a) SST k-ω (b) Tune 9.

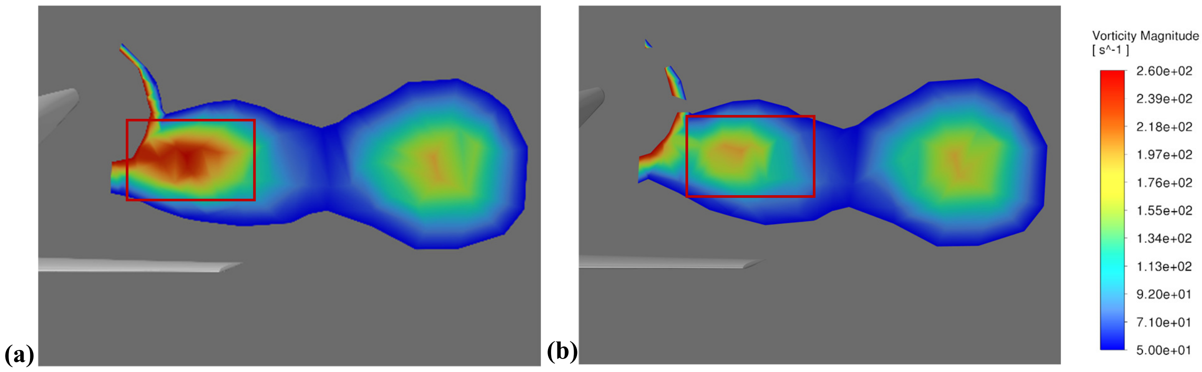

Fig. 18 Vorticity magnitude comparison on Trefftz plane 4 (a) SST k-ω (b) Tune 9.

This aligns with the what was illustrated in Section IV Part A.4, that selection of higher C_{Sep} and C_{NW} values reduces the separation extent and vortex intensity compared to the SST k-ω, and as a result, produces a lower induced drag. It also further shows that C_{Sep} is the most influential parameter in altering separation behaviour. Comparing the results in Fig. 16 for Tune 11, 12 and 16, it appears as though Tune 16 predicts a blend between Tune 11 and Tune 12. This Tune initially anticipates a higher initial induced drag as predicted by Tune 12, before predicting a sharper drop off which causes it to end in line with Tune 11's predicted end point. The main difference when comparing the tuning parameters in Table 5, is that Tune 16 has a higher C_{NW} and a lower $C_{Corn.}$ This aligns with the results derived from the flow feature studies in Section IV Part A.4, as a higher near wall parameter value and lower corner parameter value would cause the model to predict a smaller re-circulation region and reduced perturbations in the flow, which would cause a lower induced drag and a sharper negative slope.

B. Global Analysis

From Fig. 19, it can be seen that the tuned GEKO model shows a substantial accuracy increase in predicting the drag polar of the DLR F6, with four out of seven design points being within 16% of the experimental lift coefficient. Comparing this to the SST k-ω model, only two out of seven design points had a lift coefficient error less than 16%. Observing the results for the drag coefficient, for four out of seven design points, the GEKO model came within 5% of the experimental drag coefficient, which given the computational resources required to produce that result, is a significantly lower error than typically expected from RANS turbulence modelling. This proves that it is possible to utilize the GEKO model to improve the accuracy of RANS turbulence modelling for the same computational effort. To contextualize this further, a 10% reduction in predicted drag on an aircraft concept can create fuel burn reductions of 5%, mission dependent [24]. These results also validate that accuracy gains generated from tuning the model at higher AOAs will correspond to an increase in accuracy at lower, less complex flow scenarios. Looking directly at the results for each of the specific design points as in Fig. 19 below, as the AOA was raised or lowered further from the axial direction of the flow, the prediction accuracy of all models tested decreased. For the SST and the GEKO turbulence models the observed limit was 1.738° before the model's prediction accuracy for the lift and drag coefficient results for the DLR F6 significantly decreased. This result is to be expected, as increasing AOA generates progressively more complex and inherently unsteady flow structures, which are fundamentally at odds with the steady-state RANS methodology employed herein.

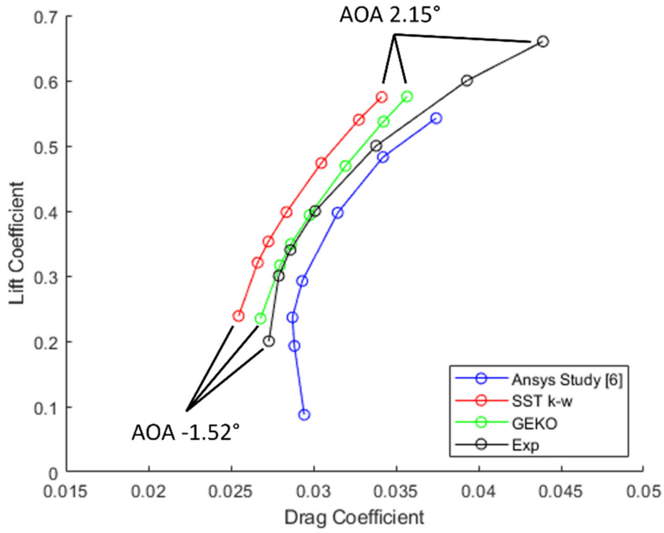

Fig. 19 Drag polar comparison for GEKO Tune 7, SST k-ω, experimental results and past ANSYS study [6].

C. Static Pressure Analysis

While the global analysis depicts a model that significantly increases the accuracy of global parameters, it is important that these improvements are further verified at a local level. Using the results from the pressure taps as discussed in Section III Part E.2 for the 1.738° AOA design point a further inspection of the flow was conducted. As shown in Fig. 20 there is a marginal improvement in the pressure curve predictions for the GEKO model (Tune 7) over the SST k-ω model. However, both models struggle to replicate the recorded values of the experimental data.

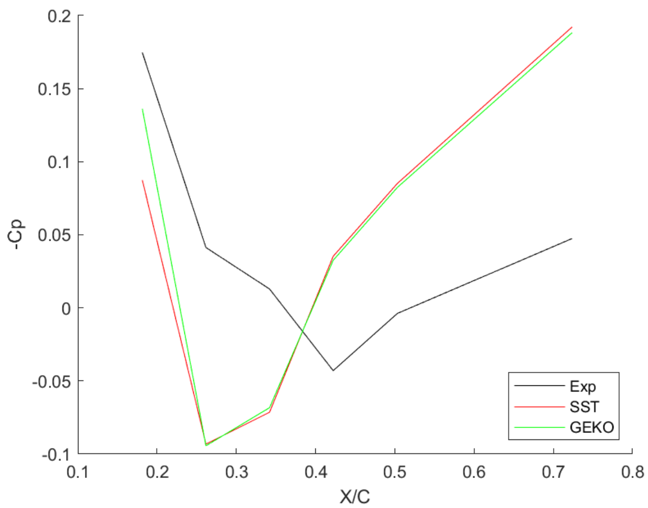

Fig. 20 AOA 1.738° pylon inboard pressure curve.

Observing the results for the pressure curve of the outboard side of the pylon in Fig. 21, it can be seen that there is a much greater improvement in both the SST k-ω and GEKO model's curve predictions. This is a result of the outboard side of the pylon featuring less complex flow features. However, it can be seen for the higher gradient location, such as, the peaks, both models struggled to resolve the full extent of the curve values. For the sudden sharp gradients, both models either over predicted the gradient causing the model's prediction to overcorrect for the pressure further downstream or the models predicted a flatter curve and failed to predict sharp gradients.

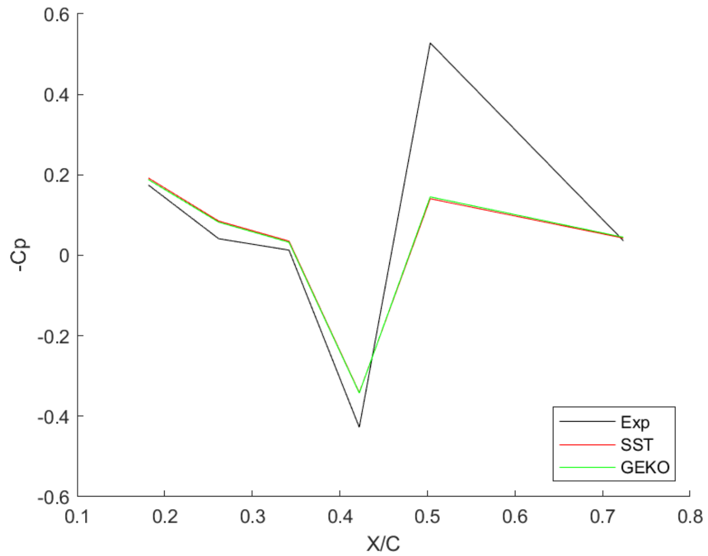

Fig. 21 AOA 1.738° pylon outboard pressure curve.

V. Conclusions

This study evaluated the GEKO model's potential to be tuned, to improve simulation accuracy both globally and locally on the DLR F6 aircraft. The work utilised available wind tunnel data from the 2nd AIAA Drag Prediction Workshop. An iterative approach was used to set computational domain dimensions, establish an unstructured meshing scheme, and to ensure the mesh quality allowed for both global and local regions to be analysed. Using a Box Behnken Design of Experiments (DoE) scheme, insights into the role of the GEKO model's free parameters, particularly C_{Sep} and C_{NW}, in altering and influencing the global performance of the DLR F6 geometry were studied. A further examination was conducted into the GEKO model's ability to modify the development of local flow features on the DLR F6 geometry, which was validated against ONERA wind tunnel data.

The findings of the study found that C_{Sep} had the most influential role in modifying the local flow features, with C_{NW}, C_{Curv} and C_{Corn}, providing the ability to further modify the flow. The work also studied the effect tuning the GEKO model had on the stability of the CFD solver. While it was illustrated that modifying the GEKO parameters had a material impact on solver stability, no direct correlation to drag prediction error was found. An analysis of the impact of tuning the model on the far field of the flow, through the use of Trefftz planes, further verified the ability of the GEKO model to modify simulation results. In this case, alterations to far-field drag were noted as being functions of increased values of C_{Sep} and C_{NW}, which was witnessed upon examination of the scale and intensity of the predicted wing-tip vortices for different parameter combinations.

This study demonstrates the potential for the GEKO model to be tuned to improve global validation performance over the SST k-ω model, with nine out of 21 tuning parameter combinations offering improvements in global performance. By completing a further fine-tuning scheme, the GEKO model's ability to be tuned within set bounds and maintain expected performance was demonstrated with 11 out of 13 tuning schemes returning a reduced drag coefficient error. These findings also verified the hypothesis of improvements generated from tuning the GEKO model at a higher AOA operating point, carry down to design points that generate a less complex flow field. In addition, observed improvements in the prediction of regions of separation / recirculating flow (in line with the experimental flow visualisation), shows that tuning / calibrating the GEKO model to match the aircraft drag polar implicitly improves the prediction of local flow features. Therefore, the modifications to the turbulence model result in alterations to the flow field that are grounded in physics, and hence give further confidence in the generalisation capability of the tuned model.

Despite the improvements to the global results and its ability to alter local flow structures to be more in line with experimental results, from the use of pressure taps along the nacelle pylon, it was found that the GEKO model could only return marginal improvements locally over the SST k-ω model, with significant discrepancies to the experimental results lingering. These results suggest that unsteady simulations are still necessary to fully capture localized flow features.

Further work in this area could pursue several different avenues. To improve the understanding and the exact influence of each GEKO parameter, a full factorial DoE scheme or machine learning enabled approach could be used to assess the influence of each parameter while the other values remain in their default state. This would allow for the individual effect of altering each parameter to be studied to verify which parameters have the greatest influence on the simulation results. Other work could investigate the use of using the same tune with other airframe geometries to investigate if improvements made from tuning on one airframe do indeed carry over to other geometries tested at similar operating conditions. This would help to further verify the GEKO model's robustness and its ability to provide improvements in performance for a range of geometries for the same operating conditions. Finally, a further study could be conducted into using the GEKO model with the aerodynamic superposition method, through separating the aircraft body and nacelle. This would evaluate the GEKO model for use in this process and assess any potential increases or decreases in accuracy that occur as a result of removing the flow interactions between the wing and pylon.

Acknowledgements

This publication has emanated from research conducted with the financial support of the EU Commission Recovery and Resilience Facility under the Science Foundation Ireland 2050 Challenge Grant Number 22/NCF/TF/10933 #NextGenerationEU.

References

[1] Aerospace America. "Symbiosis: Why CFD and wind tunnels need each other." Accessed Apr. 4, 2024. [Online]. Available: https://aerospaceamerica.aiaa.org/features/symbiosis-why-cfd-and-wind-tunnels-need-each-other/.

[2] International Civil Aviation Organization. "Report on the Feasibility of a Long-Term Aspirational Goal (LTAG) for International Civil Aviation CO_2 emission reductions.". Accessed Mar. 13, 2024. [Online]. Available: https://www.icao.int/environmental-protection/LTAG/Documents/ICAO_LTAG_Report_AppendixR1.pdf

[3] "Destination 2050." Accessed Oct. 16, 2023 [Online]. Available: https://www.destination2050.eu/.

[4] European Commission. "Towards Industrial LES/DNS in Aeronautics – Paving the Way for Future Accurate CFD." 2015. doi: 10.3030/635962.

[5] Hirsch, C. "Towards Industrial LES/DNS in Aeronautics Paving the Way for Future Accurate CFD." Accessed Jan. 23, 2024. [Online]. Available at: https://www1.grc.nasa.gov/wp-content/uploads/TILDA-Presentation-AIAA-06-2017-Web.pdf.

[6] ANSYS. "Best Practice: RANS Turbulence Modeling in Ansys CFD" Accessed Sep. 23, 2023. [Online] Available at: https://www.ansys.com/resource-center/technical-paper/best-practice-rans-turbulence-modeling-in-ansys-cfd.

[7] ANSYS. "Generalized k-ω Two-Equation Turbulence Model in Ansys CFD (GEKO)" Accessed Sep. 23, 2023. [Online]. Available at: https://www.ansys.com/resource-center/technical-paper/best-practice-geko-turbulence-modeling-in-ansys-cfd.

[8] Amstad, P., Kwok Kai So and Fischer, M. "Machine-Learning Assisted Optimization of Generalized K-Omega (GEKO) Turbulence Model Parameters for Turbocharger Radial Compressor," presented at ASME Turbo Expo 2022: Turbomachinery Technical Conference and Exposition, American Society of Mechanical Engineers Digital Collection, Oct. 2022, Volume 10D. doi: 10.1115/gt2022-78306.

[9] Gallagher, C., Stuart, C. and Spence, S. "Validation and Calibration of Conceptual Design Tool SUAVE," presented at AIAA Aviation 2023 Forum, Jun. 2023. doi: 10.2514/6.2023-3225.

[10] Lukaczyk, T., Wendor, A.D., Botero, E., Macdonald, T.L., Momose, T., Anil Variyar, J. Michael Vegh, Colonno, M., Economon, T.D., Alonso, J.C., and Orra, T.H. "SUAVE: An Open-Source Environment for Multi-Fidelity Conceptual Vehicle Design." AIAA 2015-3087, 16th AIAA/ISSMO Multidisciplinary Analysis and Optimisation Conference. June 2015. doi: 10.2514/6.2015-3087.

[11] Gatlin, G.M., Rivers, M.B., Goodliff, S.L., Rudnik, R. and Sitzmann, M. "Experimental Investigation of the DLR-F6 Transport Configuration in the National Transonic Facility (Invited)." 26th AIAA Applied Aerodynamics Conference. August 2008. doi: 10.2514/6.2008-6917.

[12] Brodersen, O. and Stuermer, A. “Drag prediction of engine-airframe interference effects using unstructured Navier-Stokes calculations.” 19th AIAA Applied Aerodynamics Conference. AIAA 2001-2414. Jun. 2001. doi: 10.2514/6.2001-2414

[13] AIAA. “2nd AIAA CFD Drag Prediction Workshop,” Accessed Oct. 14, 2023 [Online]. Available at: https://aiaa-dpw.larc.nasa.gov/Workshop2/.

[14] Bourgoin, M., Baudet, C., Kharche, S., Mordant, N., Vandenberghe, T., Sumbekova, S., Stelzenmuller, N., Aliseda, A., Gibert, M., Roche, P.-E. et al. “Investigation of the small-scale statistics of turbulence in the Modane S1MA wind tunnel.” CEAS Aeronautical Journal 9, pp.269–281, Jun. 2018. doi: 10.1007/s13272-017-0254-3.

[15] Enea.it. “ANSYS FLUENT 12.0 User’s Guide - 8.14.2 Operating Pressure, Gauge Pressure, and Absolute Pressure.” Accessed Jan. 2024. [Online]. Available at: https://www.afs.enea.it/project/neptunius/docs/fluent/html/ug/node330.htm.

[16] Rossano, V., De Stefano, G. “Testing a Generalized Two-Equation Turbulence Model for Computational Aerodynamics of a Mid-Range Aircraft.” Applied sciences, 13(20), pp.11243–11243. doi: 10.3390/app132011243.

[17] Pettersson, K., Rizzi, A. “Reynolds number effects identified with CFD methods compared to semi-empirical methods.” 25th International Congress of The Aeronautical Sciences, Vol. 3, pp.1566-1579, Sep. 2006. Available at: https://icas.org/ICAS_ARCHIVE/ICAS2006/PAPERS/540.PDF.

[18] Zore, K., Shah, S., Stokes, J., Balasubramanyam Sasanapuri and Sharkey, P. “ANSYS CFD Study for High Lift Aircraft Configurations.” 2018 Applied Aerodynamics Conference, AIAA 2018-2844, June 2018. doi: 10.2514/6.2018-2844.

[19] “Procedure for Estimation and Reporting of Uncertainty Due to Discretization in CFD Applications.” American Society of Mechanical Engineers, Journal of Fluids Engineering, 130(7), pp.078001. July 2008. doi: 10.1115/1.2960953.

[20] Celik, I., Karatekin, O. “Numerical Experiments on Application of Richardson Extrapolation with Nonuniform Grids.” American Society of Mechanical Engineers, Journal of Fluids Engineering, 119(3), pp.584–590, Sep. 1997. doi: 10.1115/1.2819284.

[21] ONERA “S2MA”. Accessed Mar. 2024. [Online]. Available at: https://www.onera.fr/en/windtunnel/s2ma-continuous-flow-wind-tunnel-variable-pressure-mach-01-mach-31.

[22] National Institute of Standards and Technology. “Comparisons of response surface designs.” Accessed Nov. 2023. [Online]. Available at: https://www.itl.nist.gov/div898/handbook/pri/section3/pri3363.htm.

[23] Houghton, E.L., Carpenter, P.W., Collicott, S.H., Valentine, D.T. “Chapter 8 - Airfoils and Wings in Compressible Flow.” Aerodynamics for Engineering Students 7th Edition, pp.525–573. Feb. 2017. doi: 10.1016/b978-0-08-100194-3.00008-0.

[24] Advisory Council for Aviation Research and Innovation in Europe. “Time for change”. Accessed Oct. 2023. [Online]. Available at: https://www.acare4europe.org/wp-content/uploads/2022/02/Time_for_change_FlightPath_2050.pdf